



The failure processes analysis of rock slope using numerical modelling techniques



S.B. Tang^{a,b,*}, R.Q. Huang^b, C.A. Tang^a, Z.Z. Liang^a, M.J. Heap^c

^a State Key Laboratory of Coastal and Offshore Engineering, Dalian University of Technology, Dalian 116024, China

^b State Key Laboratory of Geohazard Prevention and Geoenvironment Protection, Chengdu University of Technology, Chengdu 610059, China

^c Géophysique Expérimentale, Institut de Physique de Globe de Strasbourg, UMR 7516 CNRS, Université de Strasbourg/EOST, 5 rue René Descartes, 67084 Strasbourg Cedex, France

ARTICLE INFO

Keywords:

Rock slope
Slope stability
Failure process
Numerical modelling

ABSTRACT

The slope failure process includes crack initiation, propagation and coalescence during the formation of a slip surface (small deformation stage) and block movement, rotation and fragmentation during the sliding process (large deformation stage). Neither the finite element method (FEM) nor the discontinuous deformation analysis method (DDA) can solve such problems satisfactorily due to the complex mechanical behaviour of slope failure. To study the entire process of slope failure, we develop here a model that combines the FEM and DDA approaches. The main concept of this approach is to first apply FEM to model crack growth behaviour and then automatically switch to the DDA module to model the post-failure process when the slip surface forms. The efficiency and simplicity of this approach lies in keeping the FEM and DDA algorithms separate and solving each equation individually. The heterogeneous nature of the slope material at the mesoscopic level is considered by assuming that the mechanical properties of individual elements follow a Weibull statistical distribution. The slope models are progressively destabilized by the critical gravity approach, and both the failure onset and the slope collapse process are analysed. Our modelling reveals that shear cracks first initiate at the toe of slope and subsequently promote the propagation of tensile fractures due to the stress accumulation at the shear crack tips. Throughout the entire failure process, failure in tension occurs at a higher rate than shear failure and plays a dominant role in the formation of the slip surface. The effects of slope angle and pre-formed cracks on the post-failure process are studied using the proposed method. This study demonstrates that the modelling approach outlined herein is able to tackle the fundamental problems of rock slope failure and offers a better understanding of the slope failure mechanisms at both the macroscopic and microscopic levels.

1. Introduction

Landslides are a global geophysical hazard [1]. Indeed, nonseismically triggered landslides are estimated to have resulted > 30,000 fatalities worldwide between 2004 and 2010 [2]. In particular, landslides pose a significant hazard in Mainland China. Millions of landslides are located in Mainland China, and most of them are concentrated in the southern region of China (i.e., east of the Qinghai-Tibet Plateau and south of Mt. Qinling). Landslides kill hundreds of people and cost tens of billions of Renminbi (RMB) in economic losses every year. Landslide hazards have increased in China since the 1980s, likely due to increasing construction activities

* Corresponding author at: State Key Laboratory of Coastal and Offshore Engineering, Dalian University of Technology, Dalian 116024, China.
E-mail address: Tang_Shibin@dlut.edu.cn (S.B. Tang).

<http://dx.doi.org/10.1016/j.engfailanal.2017.06.029>

Received 16 November 2016; Received in revised form 2 June 2017; Accepted 14 June 2017

Available online 15 June 2017

1350-6307/ © 2017 Elsevier Ltd. All rights reserved.

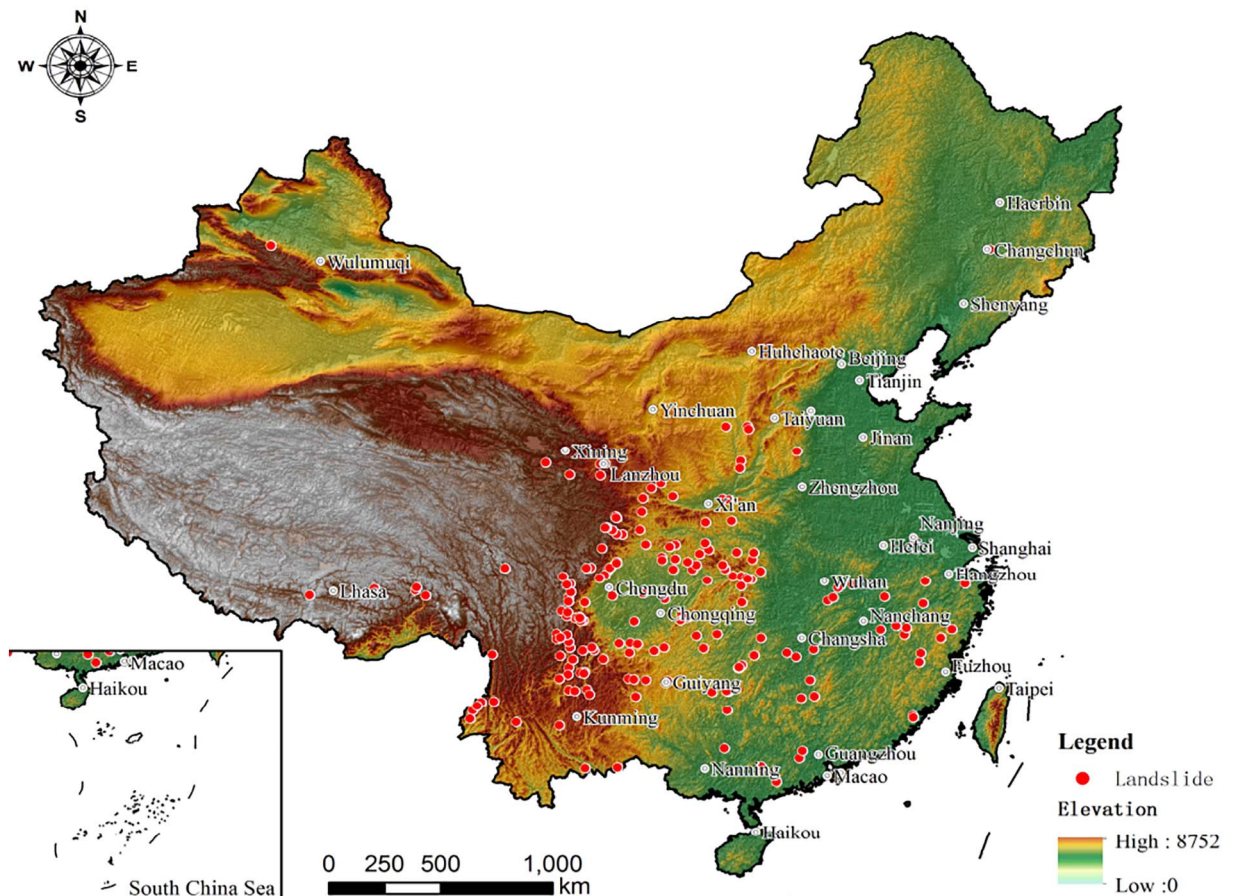


Fig. 1. Distribution of historical large-scale landslides in China.

and changes in climatic conditions [3]. For example, the Xikou landslide that occurred in the town of Xikou in Sichuan Province on July 10, 1989 was one of the most significant Chinese geological disasters of the 1980s. In this event, nearly 1,000,000 m³ of soil slid on a steep slope from a relative height of > 500 m, destroying four villages, killing 221 people, and resulting in a direct economic loss of > 6 million RMB. The landslide caused by the Wenchuan earthquake on May 12, 2008 resulted in large numbers of people dead and injured and houses destroyed. Landslides with debris volumes of > 1,000,000 m³ occurred in the town of Guanling in Guizhou Province on June 28, 2010, killing 99 people. The landslide in the city of Dujiangyan on July 10, 2013 resulted in 30 fatalities and 123 missing. In recent years, construction activities in southwest China have profoundly reduced slope stability. Following the construction of the Three Gorges Dam on the Yangtze River, > 3800 landslides were observed along the banks of this huge reservoir [4]. We have compiled here the distribution of historical large-scale landslides in China in Fig. 1.

Great efforts have been put forth to analyse the stability of rock slopes using various approaches. Current design methods can be categorized into four groups: (1) empirical design methods, (2) physical model tests, (3) limit equilibrium methods, and (4) numerical methods. In general, the stability of a rock slope can be evaluated using limit equilibrium methods, whereas complex slope deformation and failure can be analysed in depth using numerical modelling techniques. Numerical methods have been developed and applied because of their ability to better simulate actual slope failure mechanisms [5]. The finite element method (FEM) is one of the most popular methods and has been widely applied in slope stability analysis. The advantages of using FEM to study slope stability are threefold. (1) The stress-strain relation of soil or rock is considered, and thus more accurate mechanical behaviours can be computed, such as non-linear deformation and the influence of water and earthquakes. (2) No assumptions are applied in advance related to the interslide forces and their directions, or the shape or location of the slip surface. The critical slip surface is determined automatically, and the slope fails naturally [6–9] (3) Complex slope geometries can be addressed, and parametric studies can be conducted. However, many problems in geotechnical engineering involve large deformations, intact rock movement, the post-failure behaviour of a sliding slope or landslide, and the post-failure of soil due to liquefaction or debris flow. In such circumstances, FEM suffers from several disadvantages as a result of mesh entanglement, even if the updated Lagrangian method is adopted. Re-meshing might aid in resolving this problem, but the procedure is quite complicated [10]. In rock engineering, a rock mass contains many joints, faults, inclined strata, and weak zones, etc., and such discontinuities can significantly affect the mechanical behaviour of the rock mass [11]. To consider the effects of discontinuities on the behaviour of jointed rock masses, discrete numerical methods are the most popular approaches in geotechnical engineering and include the discrete-element method (DEM) proposed by Cundall and

Strack [12] and the discontinuous deformation analysis (DDA) method proposed by Shi [13]. Stead et al. [14] also discussed the developments in the characterization of complex rock slope deformation and failure using numerical modelling techniques.

Although the discontinuum-based methods can explicitly model the discontinuities present in a rock mass, they encounter difficulty in simulating failure through intact rock. The failure processes of a rock slope include not only discontinuous mechanical behaviours, but also crack initiation, propagation and coalescences. In other words, rock slope instability mechanisms occur not only along existing discontinuities but also as complex internal processes associated with shear or tensile fracture in the intact rock, particularly in massive natural rock slopes and deep engineered slopes [15,16]. Continuum- or discontinuum-based methods individually encounter obstacles in the realistic simulation of rock slope failures. Because of the Numerical Manifold Method (NMM)'s ability to address continuous-discontinuous problems, it has been successfully extended to simulate the cracking involved in rock slope failure [16–18]. Nevertheless, although NMM has shown unprecedented success in accurately modelling both continuous and discontinuous mechanical behaviour of a rock mass, it suffers from certain difficulties, such as linear dependence and “geometrical” ill-conditioning [19]. Furthermore, the calculation speed, parallel computing and programmability, and richness of the existing NMM code cannot compete with that of the FEM in the current state-of-the-art. Indeed, many popular and successful FEM programs are widely available that can be used in coupling analysis. Therefore, many studies have combined the advantages of the FEM and DDA methods to efficiently simulate crack propagation processes. Bao and Zhao [20], for example, presented a hybrid approach for two-dimensional problems that takes advantage of both FEM and DDA to solve problems involving continuum and discontinuum domains. Chen and Zhang [21] introduced a technique that coupled FEM and DDA and applied it to selected examples to demonstrate the effectiveness of the proposed coupling method. Shyu [22] performed numerical simulations to demonstrate the improvement and flexibility achieved if a finite element approach is associated with DDA to handle discontinuous contact problems under large displacements and deformations. Choo et al. [23] extended the hybrid FEM and DDA method to model hydraulic fracture, the results of which appear to be consistent with existing theories of hydraulic fracture mechanisms. Although hybrid DDA/FEM significantly improved the capability of DDA, it becomes computationally expensive for problems that involve large numbers of blocks. Furthermore, because of the lack of effective crack growth simulations, previous studies are difficult to apply to practical rock engineering problems. Therefore, the aim of this study is to propose a new combined FEM and DDA method that can model the failure of rock slopes. The first portion of the paper presents the outline of the combined method, including the theory of fracture initiation, propagation and coalescence in intact rock, and the strategy of combining the FEM and DDA methods. Simulations and experimental tests are subsequently conducted for model validation. The slopes are destabilized progressively under a critical gravity condition, and the failure processes and mechanisms are investigated using the numerically obtained information.

2. Outline of the combined method

2.1. Methodology of combined FEM and DDA

By coupling the FEM and DDA methods in the program for the rock failure process, the advantages of each method are leveraged, and the disadvantages are reduced or even eliminated. Two types of program coding methods exist for coupling analysis: (1) design using shared variables and (2) design using exchanged data. In the first type, all of the methods are coded in one program, and each module/method shares the variable names in memory, i.e., the variable names and the grammar of the program code are held consistent, and the equations of each module method are solved in a dependent manner. The limitation of this approach is that the coding is complicated, and the coupled program cannot be easily linked with other existing programs. The second method is known as the independent module method in which two independent modules (two different programs written in different languages or as different available programs) exchange information with each other via data files. This method is easy to program, requires less computer memory, and many existing software packages can be used in the coupling analysis without major modification. A batch program is required to control this process, i.e., when one program ends, the other program should begin with the exchanged data file. The second approach consumes a greater amount of time for saving and reading the data exchanged between FEM and DDA. However, with the development of new computer technology, especially the development of solid-state drives, the time consumed in saving and reading the exchanged data from the files is considerably shortened. In this study, the second approach is used in the coupling of FEM and DDA.

In general, post-failure analysis of slope deformation, including block movement, contact and detachment, is a time-consuming process. Although any time-step size can be theoretically used, due to DDA's implicit methodology, small strain-based formulation, and open-close iterations that satisfy the no-penetration and no-tension contact constraints, the time-step size in practice is restricted to a size that is not significantly larger. DDA uses an implicit time-marching scheme that is unconditionally stable. However, it requires a number of open-close iterations in each time step to satisfy the contact constraints and a linear system of equations must be solved in each iteration, which makes it computationally much more expensive per time step. Therefore, the coupled FEM/DDA method is also a time-consuming process for studying the failure process of a rock slope. However, the analysis process can be further simplified according to the failure characteristics of the rock slope. The rock slope failure process can be divided into two stages: (1) the formation of the shape or location of the slip surface and (2) the movement of separated rock blocks. The first stage includes crack initiation, propagation, and coalescence processes, which require small deformations and can be modelled using FEM. In the second stage, rock blocks move along the formed slip surface (post-failure stage), which requires large deformations and a dynamic method such as the DDA method to model the mechanical behaviour. Therefore, in this study, an alternative simplified approach for fully deformable blocks was developed. The new approach simplifies the combined DDA-FEM method by applying FEM and DDA in different failure stages during the failure of the rock slope, i.e., FEM is used in crack initiation, propagation, and coalescence

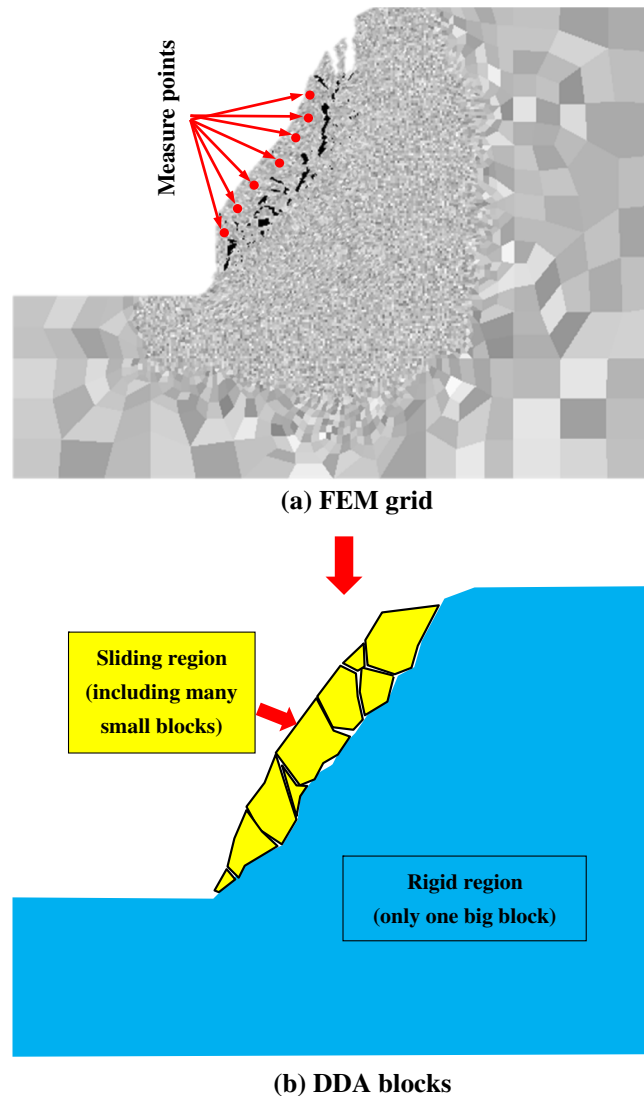


Fig. 2. Schematic of the combined FEM and DDA method. (For interpretation of the references to colour in this figure, the reader is referred to the web version of this article.)

processes prior to formation of the slip surface, and DDA is used in the post-failure process. The critical slip surface is determined automatically first by FEM, and the DDA module is subsequently invoked.

We note that the joints and faults in a rock slope can be modelled as small and weak solid elements in FEM because of the small deformations in the first stage of rock slope failure. It is important to determine when to automatically call upon the DDA module. In other words, we need to know when the slip surface has been formed so that we can switch from the FEM modelling to the DDA module. During the first stage of rock slope failure, crack growth (including crack initiation, propagation, and coalescence processes) is the dominant failure feature. When the slip surface forms, the rock slope is split into two components: (1) the sliding region and (2) the rigid region, as shown in Fig. 2(a). A clear difference between the sliding and rigid bodies is the displacement of movement, i.e., the movement of elements in the sliding region is significantly larger than that of the rigid region. This information can be used to determine whether a sliding surface has formed, similar to the measurement of surface displacement and deformation of mass movements by high resolution satellite and aerial images [24,25] or radar monitoring [26]. By setting many measurement points near the surface of the rock slope (the red dots in Fig. 2(a)), it is easy to monitor the displacement increment of the slope. When the displacements of the measured points suddenly increase, the FEM module can assign the elements that belong to the sliding region according to the large displacement criterion. The FEM module then prepares the data for the DDA module (including block information, displacement and force, mechanical properties) and invokes the DDA module to address the large displacement analysis, block contact, and block movement of the sliding mass. A sketch of the transition from the FEM results to the DDA module is shown in Fig. 2(b), where the yellow-coloured blocks represent the sliding mass, and the blue-coloured block indicates the rigid region. We propose here a strategy for the transfer of FE data to the DDA module to more efficiently model the post-failure behaviour of the rock

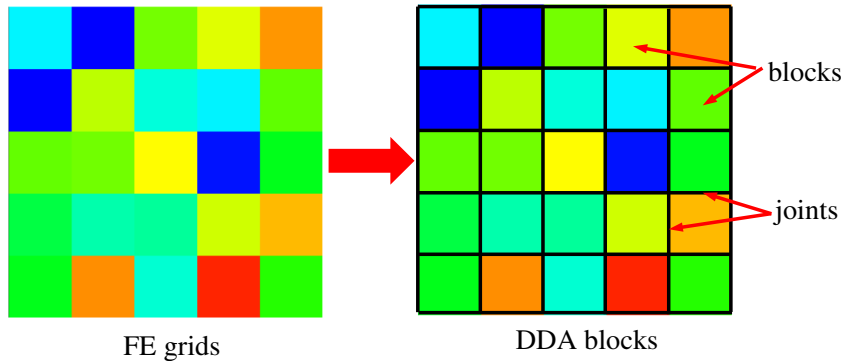


Fig. 3. Schematic of the transformation of FE grids to DDA blocks. The DDA blocks are separated by joints.

slope failure. During the transfer, all of the FE grids in the rigid region are merged into a large block, whereas the grids in the sliding region are consistent between the FE and DDA, i.e., each element in FE is considered as a single DDA block. The boundary of the large block is fixed. The benefit of this approach is a significant reduction in the number of blocks in the DDA modelling. Therefore, in the first stage of slope stability analysis, the rock slope can be divided into additional elements to more accurately simulate the potential slip surface. In the second stage, the joint lines in the sliding region are inherited from the FE grid for DDA modelling, i.e., each element in FE is mapped to a DDA block, and the edges of elements are translated to the joints around the blocks (see Fig. 3). The physical and mechanical properties of the joints (friction angle (φ), cohesion strength (c) and tensile strength (σ_t)) in each DDA block are consistent with the FE elements. Note that if any elements failed during FE modelling, the joint properties (including φ , c and σ_t) are set to zero. A flow chart of the combined FEM and DDA method is shown in Fig. 4, which shows that FEM and DDA modules are independent each other and need only to transfer data. Since the FEM and DDA modules are independent from one another, the convergence of the proposed numerical model depends on the convergence of the FEM and DDA module. The FEM modelling of the failure process (crack initiation, propagation and coalescence) is converge as verified by comparison with experiments and engineering-scale observations [27,28]. For the DDA method, it is a mathematical convergence method [13]. We further note that the transference of parameters from FEM to DDA does not result in a convergence problem. Therefore, our proposed approach does not suffer any problems associated with convergence.

2.2. FEM method for modelling of cracking

Terzaghi [29] and Einstein et al. [30] suggested that the failure of a rock slope requires a complex interaction between pre-existing discontinuities as well as crack initiation and propagation through the intact rock. Generally, as mentioned above, the crack initiation, propagation, and coalescence process is the dominant mechanical behaviour prior to slope sliding, as addressed in the modelling by Wong and Wu [16], Jiang et al. [5] and Scholtès and Donzé [31]. Most previous studies have assumed that pre-existing cracks exist within in the rock slope, and the crack growth and coalescence processes were subsequently modelled. Furthermore, previous studies also assumed that rock is a homogeneous material and that cracks only occur at high-stress locations such as at crack tips. However, rock is typically a heterogeneous material, and the heterogeneity of rock causes non-homogeneous stress distributions, causing particularly large tensile stresses [28,32]. In the current study, the heterogeneity of rock at the mesoscopic level is assumed to conform to a Weibull distribution, as defined by the following probability density function:

$$\varphi(\alpha) = \frac{m}{\alpha_0} \left(\frac{\alpha}{\alpha_0}\right)^{m-1} \cdot e^{-\left(\frac{\alpha}{\alpha_0}\right)^m} \tag{1}$$

where α is a given mechanical property (such as strength), α_0 is the scale parameter and m is the shape parameter that defines the shape of the distribution function. In the current study, the parameter m defines the degree of material homogeneity and is thus referred to as the homogeneity index. Weibull distributions have been shown to well describe rock heterogeneity in previous modelling studies [33–35].

The rock slope is discretized into many small elements that are assigned mechanical properties according to Eq. (1). Each small element follows the following assumptions: (1) rock is a brittle-elastic material with residual strength, and its mechanical behaviour can be described by the elastic damage constitutive law; (2) elements fail (tensile or shear) when the failure criterion is reached, and the element stiffness degrades as elements fail. In this study, the Mohr-Coulomb relation with a tensile cut-off criterion is adopted for the elements. Damage occurs in elements when the local stresses reach the tensile or shear strength of the material.

Taking into account the “modified effective stress” concept, we introduce the damage variable d ($0 \leq d \leq 1$). This parameter measures the reduction of resistant areas due to crack initiation and propagation, which can be expressed as

$$\sigma = E_0(1 - d)\varepsilon \tag{2}$$

where σ and ε are the stress and strain tensors, respectively, and E_0 is the stiffness matrix. The evolution of the damage parameter d can be found in Tang and Tang [28] and Tang et al. [36].

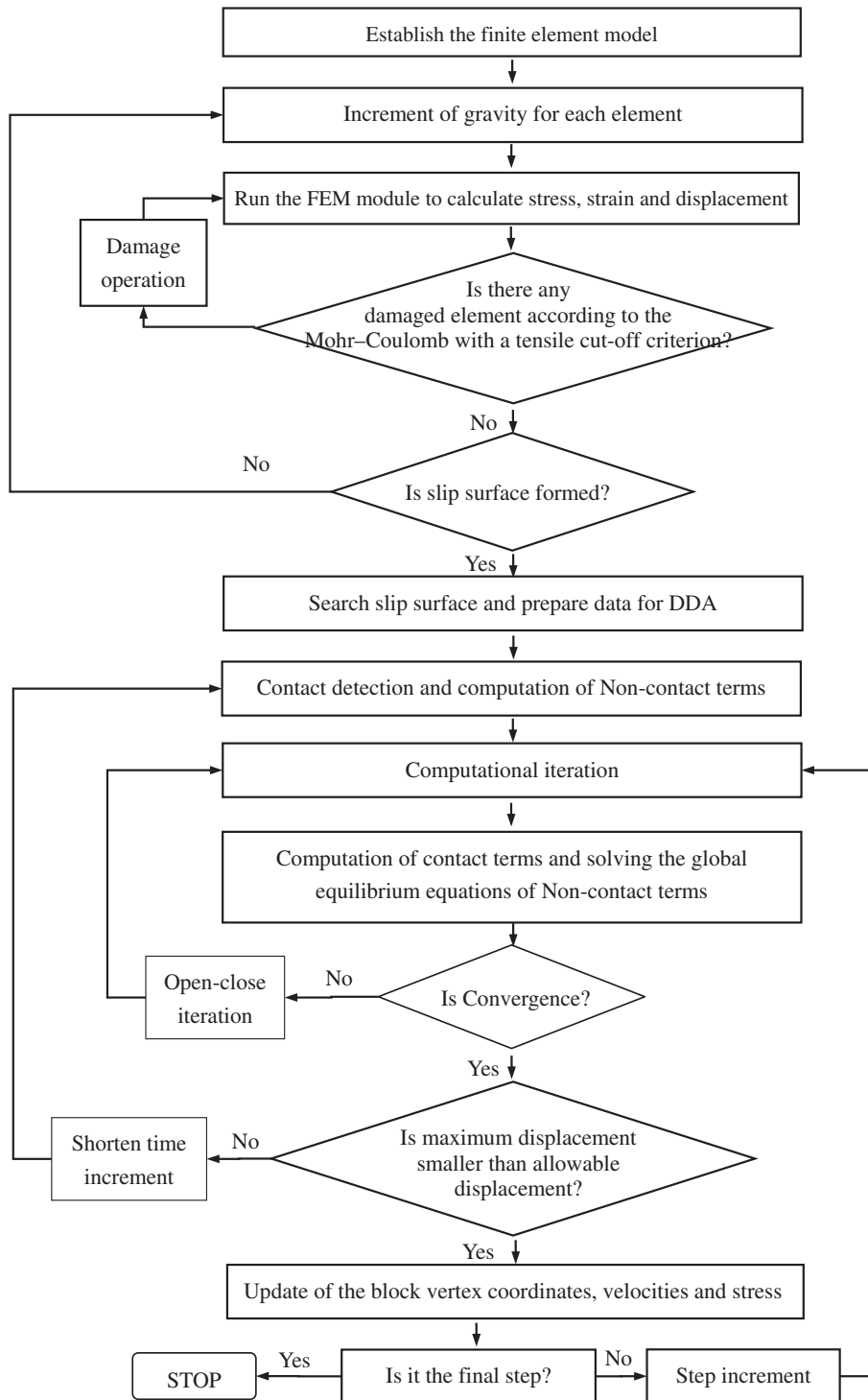


Fig. 4. Flow chart of the combined FEM and DDA method.

The relatively small dimension of the generated rock slope samples in addition to the high strength of the material could result in a stable condition of the slope under a normal gravity environment. The gravity increase method [5,37] and strength reduction method [31,38] are considered the most widely used methods. Scholtès and Donzé [31] demonstrated that the same results can be obtained using both techniques. In the gravity increase method, gravity forces are increased gradually until the slope fails, and the factor of safety is defined as the ratio between the gravitational acceleration at failure (g_f) and the actual acceleration due to gravity

($g_0 = 9.8$ for Earth), i.e., $SF = g_f/g_0$. In this paper, the slope stability is studied using the gravity increase method. In each step, the gravity of the rock slope model is first increased, and the damage caused by increasing gravity is subsequently computed according to the damage evolution law proposed by Tang and Tang [28] and Tang et al. [36]. The displacements of the measurement points shown in Fig. 2(a) are assessed to determine whether the slope exists in unstable deformation (the transition to instability, in our model, is when there is sudden, and significant, increment of displacement). This process is repeated as the gravity is increased in a step-by-step manner until the displacement of these measurement points suddenly increases, and that level of gravity is treated as the critical gravity.

After the numerical sample with the appropriate boundary conditions is established, the finite element method (FEM) is then used to analyse the stress and strain and the temperature distributions in 2D using 4-node quadrilateral elements. As soon as strain (ϵ) and stress (σ) distributions at each time step are obtained by the FEM, the damage module is run to determine whether any damage occurred in any of the meso-elements and to address such damages based on Tang and Tang [28] and Tang et al. [36]. Subsequently, the stress and deformation distributions throughout the sample are adjusted instantaneously to reach a new equilibrium state by re-computing the numerical sample with new parameters and without any further loading. Such a process (damage operation and re-computing) is repeated in each step until no further elements are damaged, after which the next external loading increment is applied. Damage propagates into the adjacent elements during such a process. The coalescence of these meso-damages gradually forms macrocracks that, eventually, conspire to form the slip surface of the rock slope.

2.3. DDA method for sliding

The DDA method is a large deformation and displacement method that is suited for studying of rock instability. DDA uses a finite element-type mesh, but all of the elements are isolated blocks bounded by pre-existing discontinuities. Therefore, a finite element mesh is easy to switch to DDA input data. When the blocks are in contact, Coulomb's law applies to the contact interface, and the simultaneous equilibrium equations are formulated and solved for in each loading or time increment. DDA considers both static and dynamic behaviour using a time-step marching scheme and an implicit algorithm formulation. The difference between static and dynamic analysis is that the former assumes that the velocity is zero at the beginning of each time step, whereas the latter inherits the velocity of the previous time step. By adopting first-order displacement approximations, the DDA method assumes that each block contains constant stresses and strains throughout. The behaviour of any point within a block can be described using six variables: two translation terms, one rigid region rotation term, two normal strain terms and one shear strain term [13,39]:

$$\begin{pmatrix} u \\ v \end{pmatrix} = [T_i][D_i] = \begin{bmatrix} 1 & 0 & -(y - y_0) & (x - x_0) & 0 & (y - y_0)/2 \\ 0 & 1 & (x - x_0) & 0 & (y - y_0) & (x - x_0)/2 \end{bmatrix} \begin{Bmatrix} u_0 \\ v_0 \\ r_0 \\ \epsilon_x \\ \epsilon_y \\ \gamma_{xy} \end{Bmatrix} \quad (3)$$

where u and v are, respectively, the displacement of any point within the block in the X and Y directions; x_0 , y_0 and z_0 are the coordinates of the block centroid; x , y , z are the coordinates of an arbitrary point within the block; u_0 and v_0 are the block translations in the X - and Y -directions, respectively; r_0 is the rigid region rotation in the radius; and ϵ_x , ϵ_y and γ_{xy} are the normal and shear strains of the block, respectively. For more details about the theory and the implementation of numerical method, please refer to Shi [13] and Shi and Goodman [39].

3. Modelling the rock slope failure process

The geometry of the excavated slope model studied in this paper is shown in Fig. 5. Importantly, this geometry is the same as that used in the experiments of Zhang et al. [40]. If we consider the same material here, the elastic modulus, tensile strength and Poisson's ratio in the numerical specimen should be 50 MPa, 5 kPa and 0.32, respectively. The cohesion and friction angle are taken as 40 kPa and 32° , respectively. The left and right boundaries of slope are fixed in the x -direction but the y -direction is free, whereas the bottom boundary is fixed in the y -direction but free in the x -direction.

3.1. Formation of a slip surface

Fig. 6 shows the failure pattern of the rock slope modelled by FEM when the slope angle α is 75° . It was noted in Section 2.1 that the displacement of the slope is relatively small before the sliding surface forms. Indeed, only minor damage (cracks) can be observed during the initial stages of slope failure in our numerical model (Fig. 6(a)), in agreement with observations from both experimental investigations and geological surveys. Fig. 6(a) shows that a long crack formed at the top of the slope, and that a few smaller cracks formed within the slope and at the toe of the slope. Importantly, the long crack at the top of the slope has a surface expression (i.e. visible at the surface), while the smaller cracks, even those at the toe of the slope, do not break the surface (Fig. 6(a)). The numerical result agrees with the in-site observations that, prior to a landslide, many slopes display surface cracks at the top of the slope (as shown in Fig. 7) but few visible cracks at the toe of the slope. Generally, shear cracks occur near the toe of the slope, and tensile cracks initiate at the slope crest. Shear fractures are unlikely to produce visible cracks because the slip surfaces remain in contact. Tensile failures (i.e. opening-mode fracture), however, result in fracture surfaces that separate and are therefore easily observed (Fig. 7). One

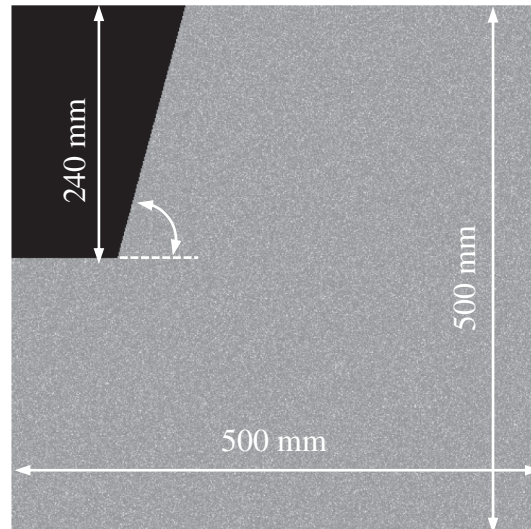


Fig. 5. The geometry of the modelled slope. The slope angle is given by α .

of the advantages of numerical modelling is can provide images of the slope at progressively higher displacements, which makes it easy to follow the progression of slope failure. Fig. 6(b) and (c) show the same slope as in Fig. 6(a) but the displacement has been enlarged 10 and 50 times, respectively. The image of Fig. 6(c) shows that the sliding surface has formed and has divided the slope into a sliding region and a rigid region. As explained above, the large displacement and movement of the sliding region must be subsequently studied using the DDA module.

Fig. 8 shows the displacement distribution during failure of the 75° -angle slope. The displacement is normalized in each step to highlight the largest displacement area (warm colours indicate high-displacement and cold colours indicate low-displacement). The results indicate that, when the gravitational acceleration is relatively small (i.e. $19g_0$), the largest displacement area is located at the top-right corner, and the smallest displacement is located at the bottom of the slope. With each additional increment of gravity, the zone of largest displacement is gradually transferred to the sloping sides, such as when $g = 30g_0$ (Fig. 8). When g increases to $37g_0$ or $40g_0$, the largest displacement area is mainly concentrated in the vicinity of the sloping sides, but it is difficult to judge from these images whether the slope is unstable. Further increments of gravity accelerate the localization of the large displacement, which can be clearly observed when $g = 45g_0$. Finally, the largest displacement is concentrated only near the sloping sides when $g = 49g_0$. To better understand whether the slope has transferred into an unstable state, we use the model to plot the displacement vector fields for the slope. The displacement vector fields for $g_f = 48g_0$ and $g_f = 49g_0$ show that there is a sudden increment of displacement in the sliding region at $g_f = 49g_0$ (Fig. 9), indicating that the critical gravitational acceleration of this slope model is $g_f = 49g_0$.

Fig. 10 presents the simulated initiation, propagation, and coalescence of the fractures in the slope model for increasing gravitational acceleration steps, and Fig. 11 presents the corresponding stress distribution throughout the numerical slope. The results indicate that cracks initiate first at the toe of the slope and propagate upward along the slope (i.e., $30g_0$ and $35g_0$) (Figs. 10 and 11). Fig. 12 shows the types and locations of failures that occurred during increasing increments of gravitational acceleration. Fig. 12 shows that both tensile (red circles) and shear failures (blue circles) occur in the heterogeneous material, which agrees with the

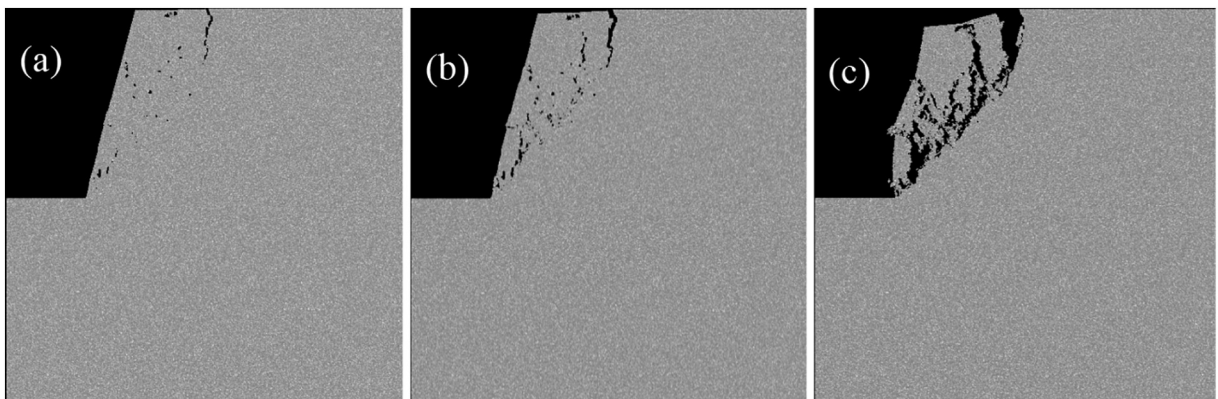


Fig. 6. The failure pattern of the rock slope modelled by FEM for a slope angle of $\alpha = 75^\circ$, where (a), (b) and (c) show images of the sliding region with displacement enlarged to 1, 10 and 50 times, respectively.



Fig. 7. In-site observation of surface cracks at the top of a slope.

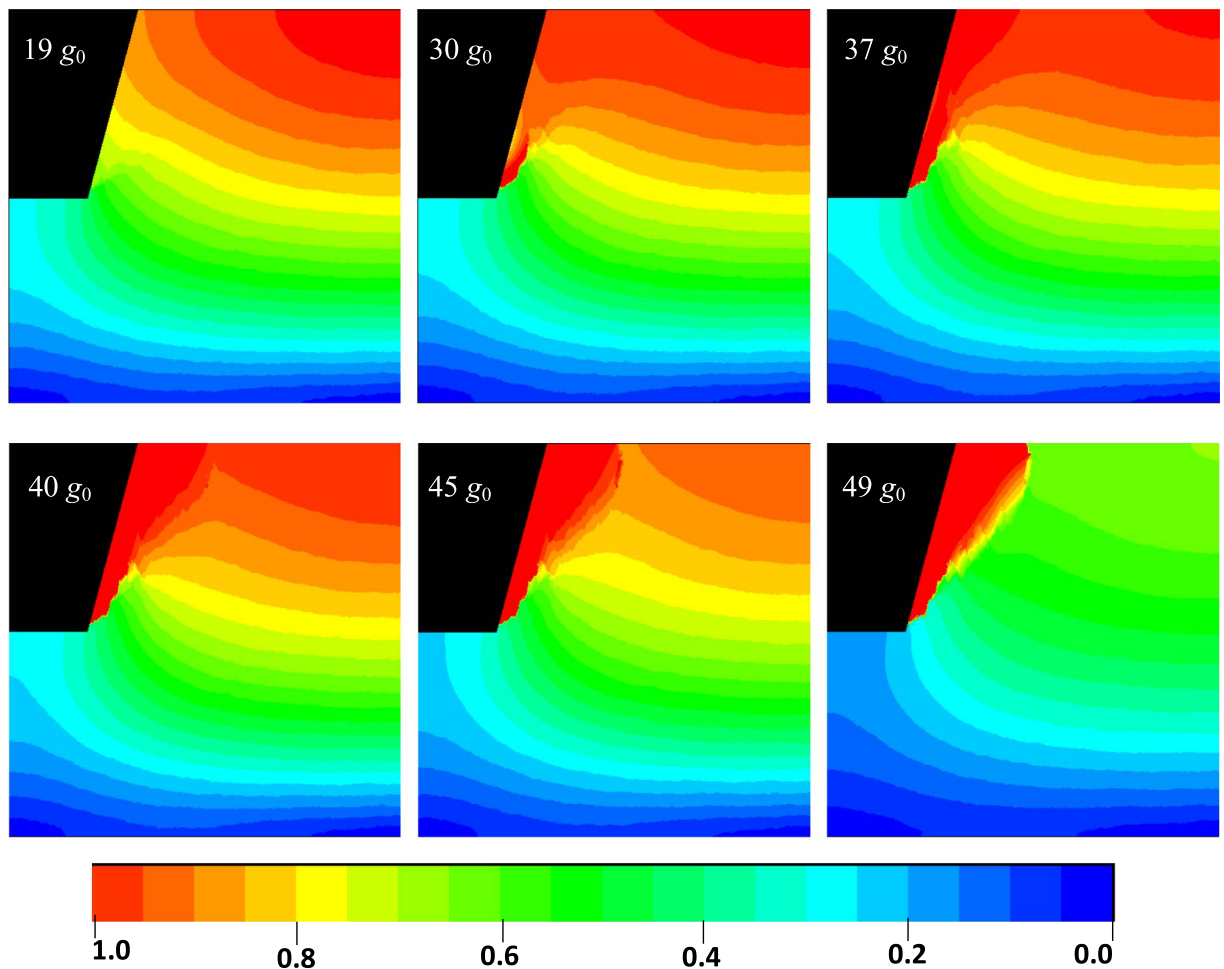


Fig. 8. The evolution of displacement in a slope with a slope angle of $\alpha = 75^\circ$ at different gravity step increments, from $19g_0$ to $49g_0$. The colour bar shows the normalized displacement in each gravity increment step. Warm colours indicate high-displacement and cold colours indicate low-displacement. (For interpretation of the references to colour in this figure legend, the reader is referred to the web version of this article.)

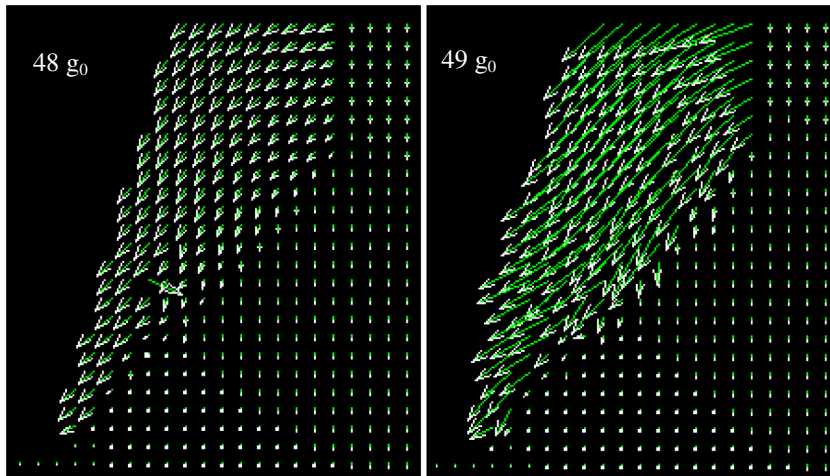


Fig. 9. Displacement vector evolution of the slope ($\alpha = 75^\circ$) at $g = 48g_0$ and $g = 49g_0$. The arrow direction and size represents the direction and size of the displacement, respectively.

finding of Pells [32] that non-homogeneity in the material itself can lead to non-uniform stress across the section. Due to the effect of heterogeneity on mechanical behaviour, microfailures (i.e., fractures at a length scale much shorter than the eventual slip surface) can occur at locations of high-stress, and also initiate at weak locations due to the presence of local discontinuities. The stress distribution in Fig. 11 further indicates that the heterogeneity of the rock causes non-homogeneous stress to be distributed throughout the slope, causing particularly large stress fluctuations that result in distributed failures at the beginning of loading, as shown in Fig. 12, where many isolated shear fractures form at the toe of the slope (i.e., at $15g_0$). With further increments in loading, the number of shear failures (blue circles) increases, and tensile failures (red circles) occur in the regions where shear failures have been generated (i.e., $20g_0$ and $25g_0$, as shown in Fig. 12). Many tensile failures are generated when $g = 30g_0$, which results in an

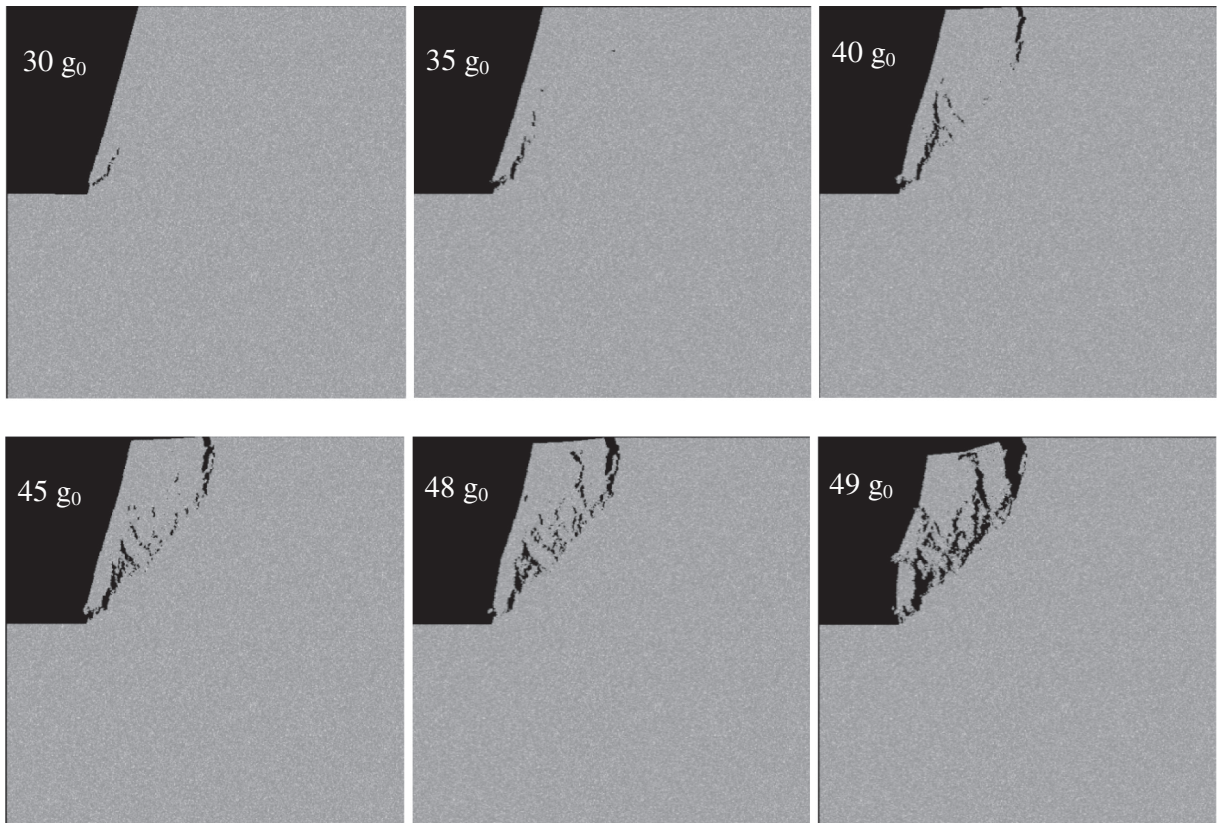


Fig. 10. Images of the failure process of a slope with a slope angle $\alpha = 75^\circ$ at different gravity step increments, from $19g_0$ to $49g_0$.

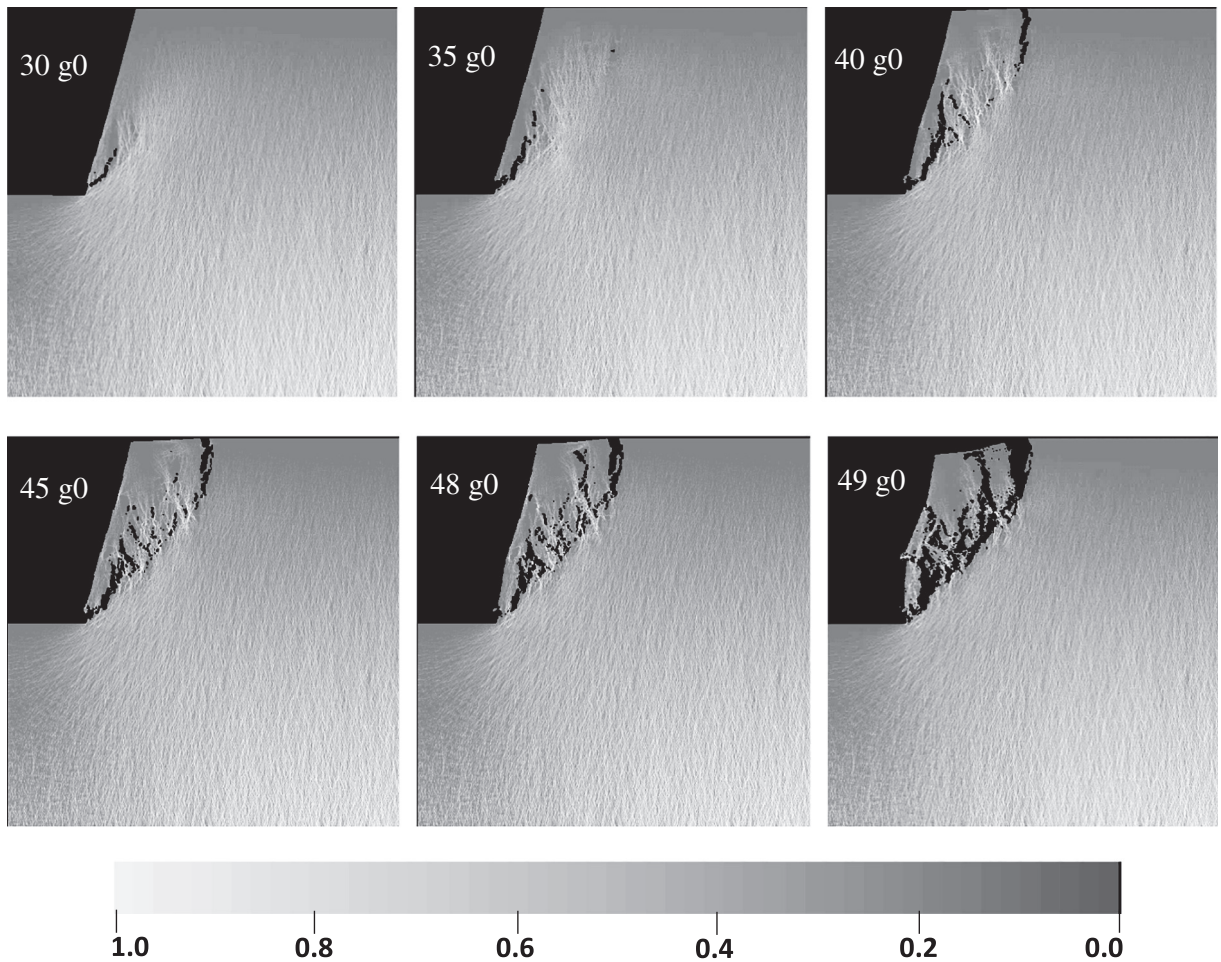


Fig. 11. Images showing the evolution of shear stress with in a slope with a slope angle of $\alpha = 75^\circ$ at different gravity step increment, from $19g_0$ to $49g_0$. The colour bar shows the normalized shear stress in each gravity increment step. Bright colours indicate high-stress and dark colours indicate low-stress. (For interpretation of the references to colour in this figure legend, the reader is referred to the web version of this article.)

observable crack at the toe of the slope, as shown in Figs. 10 and 11. Tensile failures begin to localize and finally lead to the formation of macrocracks. It is interesting to note that when gravitational acceleration increases to a certain value (such as $40g_0$), a crack appears in the top of the slope (see Figs. 10 and 11), similar to that shown in Fig. 7. The failure types shown in Fig. 12 indicate that such surface cracks are caused by the initiation and propagation of tensile failures (red circles).

The failure types and locations shown in Fig. 12 facilitate a deeper understanding of the mechanism of the slope. The failure process indicates that shear failures (blue circles) occur at the slope toe, which in turn cause load transfer to the adjacent areas (such as at $15g_0$). Because of the heterogeneity of rock, shear failures are scattered near the toe of the slope. According to fracture mechanics, stress concentrates at the tip of an existing shear crack and likely leads to crack extension due to tensile stresses. For this reason, tensile failures (red circles) appear in the region where earlier shear failures occurred, as shown in Fig. 12 when $g = 20g_0$. As loading progresses (i.e., $g = 25g_0$ and $30g_0$), shear failures occur closer and closer to the top of the slope. At the same time, tensile failures are also produced in the shear failure region near the slope toe. The number of shear failures is larger than of the number of tensile failures at the beginning of loading, but the opposite situation occurs when the loading increment reaches a certain value, such as $35g_0$. With subsequent loads, shear failure may continue to occur, but tensile fracture is the main type of failure in the slope, especially in the region of the top surface. The coalescence of mixed tensile-shear crack development from the toe of the slope and tensile crack development from the upper surface results in a sliding resistance force that is lower than the sliding force and subsequently leads to slope-scale instability. It can be observed that the cracks that form between the tensile-failure clusters at the top and the toe of the slope are mainly attributed to shear failure, as shown in Fig. 12 when $g = 40g_0$ (the shear failure coalescence region is indicated by a dashed green line). This coalescence region is also observed in the stress distribution shown in Fig. 11, which shows that large shear stresses (indicated by brighter colours) are concentrated in the coalescence region. The failure process of the slope indicates that both tensile failures and shear failures must be implemented in the numerical model to more deeply understand the failure mechanism of different slopes.

Fig. 13 presents the different failure patterns of slopes with different slopes angles (45° , 75° and 85°). It can be observed that the

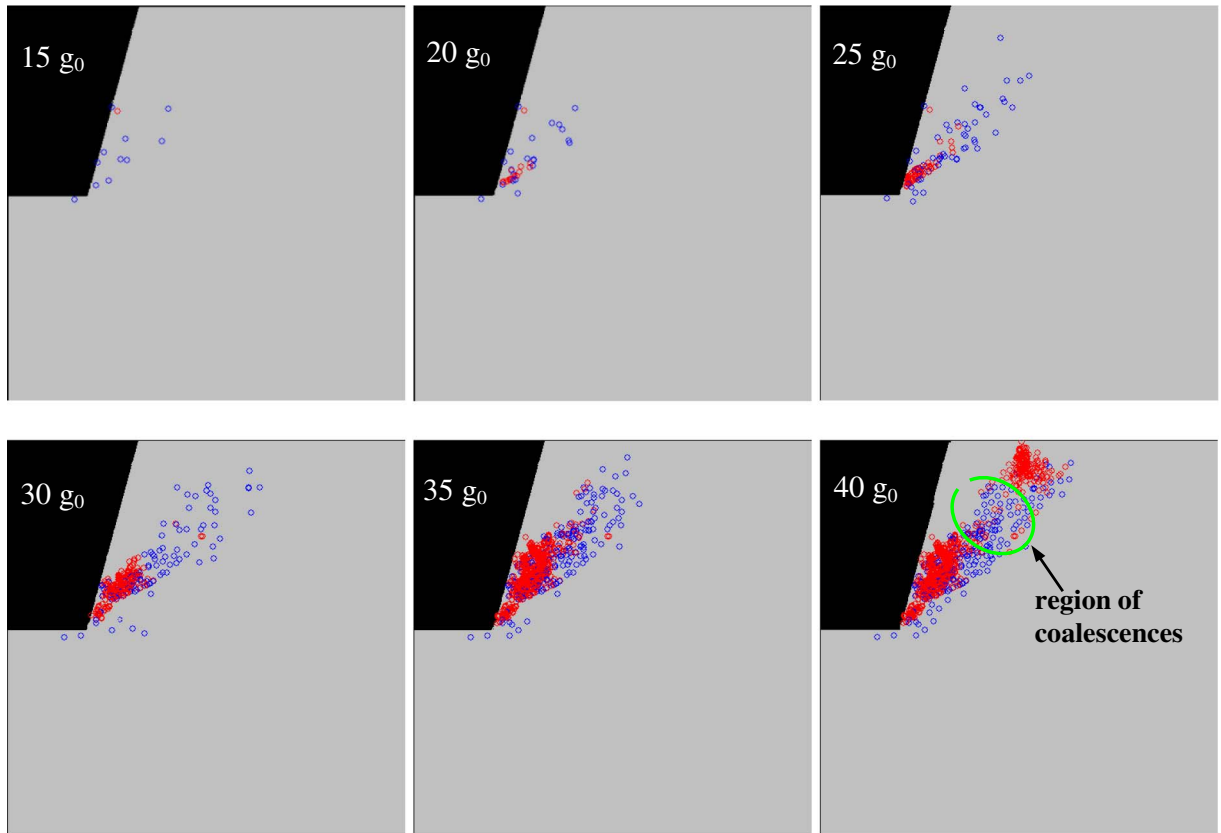


Fig. 12. Images showing the location of tensile (red circles) and shear (blue circles) failure events within a slope with a slope angle of $\alpha = 75^\circ$ at different gravity step increments, from $15g_0$ to $40g_0$. The green dashed line shows region of shear-failure coalescence. (For interpretation of the references to colour in this figure legend, the reader is referred to the web version of this article.)

cracks tend to initiate from the slope toe when the slope angle is relatively large. When the angle is smaller, the cracks are more likely to start above the slope toe. Fig. 14 shows the experimentally obtained failure patterns of a slope when the slope angle is 85° , taken from the work of Zhang et al. [40]. The final gravitational acceleration required for slope failure in the experiment was $45g_0$. The critical slip surface obtained from our numerical modelling agrees well with that observed in the experiment of Zhang et al. [40] (similar findings were also reported in Hu et al. [41]). In both the numerical and experimental results, tensile fractures were observed at the top of the slope, which agrees with the common failure mode for full-scale in-situ slopes (as shown in Fig. 7).

3.2. Large displacement and block movement modelling of the slope

As soon as the slip surface forms in the slope, the sliding region will experience large displacements and block movement. Figs. 2

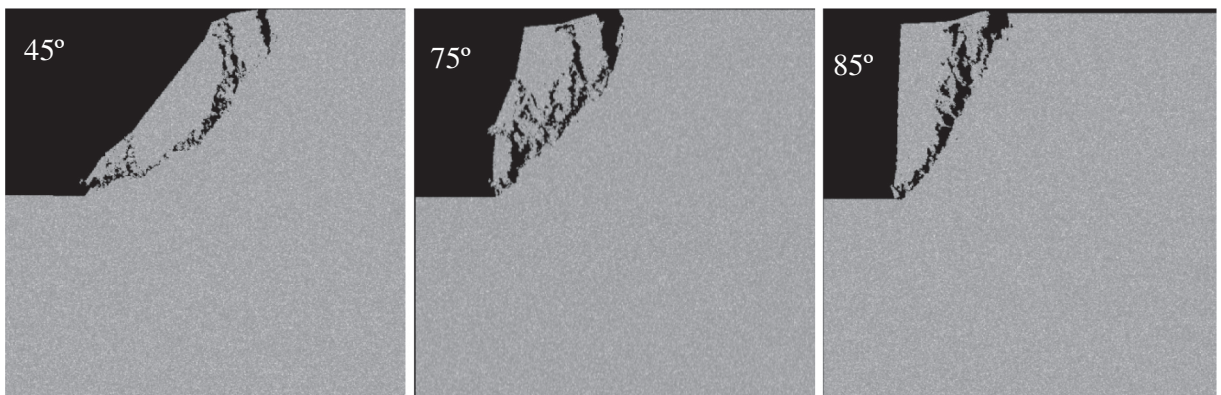


Fig. 13. Slope failure patterns in slopes with different slope angles (displacement enlarged 50 times).

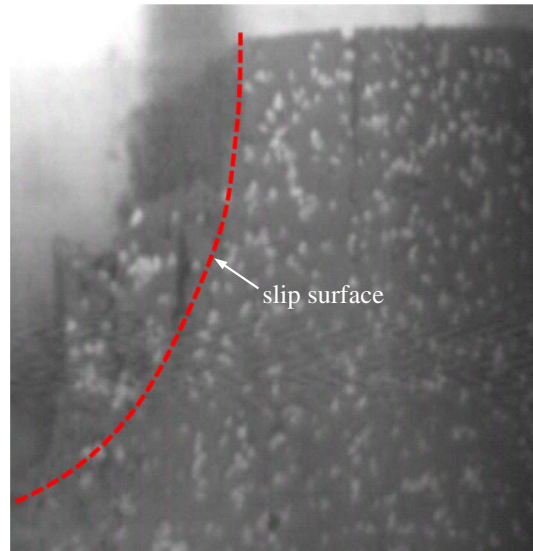


Fig. 14. Photograph of an experimentally obtained slope failure patterns for a slope with a slope angle of 85° [41].

and 4 show that the DDA module is invoked to address the mechanical behaviour in the post-failure slope. Jing [42] noted that the chief disadvantage of DDA is the requirement of knowing the exact geometry of the fracture systems in the problem domain. However, when the DDA geometry is inherited from that of the FEM grid, especially when the FEM module automatically delineates the slip surface, the DDA method is more convenient for modelling the post-failure process of the slope. In this study, when the FEM module prepares data for DDA module, the friction angle, cohesion and tensile strength of new cracks are assumed to be zero, and other joints (element edges shown in Fig. 3) are consistent with the elements. Only gravitational loading is applied to the slope, which is equal to the gravitational acceleration at failure. Fig. 15 shows the input geometry in DDA modelling of the post-failure slope with an initial slope angle $\alpha = 75^\circ$ in which the sliding region includes 16,451 small blocks (elements). The post-failure process of this slope modelled by the DDA module is shown in Fig. 16 in which the large-scale movement and rotations of blocks are clearly demonstrated. This type of deformation mode is highly difficult to simulate by conventional FEM or other continuum-based numerical methods. The result shows that the sliding region moves along the slip surface (see Fig. 16(a)) at the beginning of sliding. With further landslide progression, the sliding region is divided into many blocks, including large and small blocks (Fig. 16(b)). We note that most of the small blocks are mainly distributed near the slip surface. These small blocks are elements that failed during the

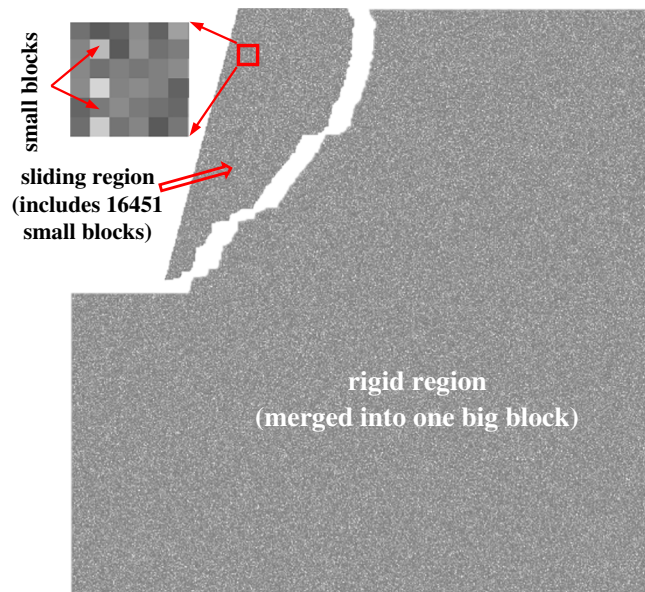


Fig. 15. Input geometry for the DDA modelling. Example shown is the post-failure slope configuration for a slope with an initial slope angle $\alpha = 75^\circ$, as provided by the FEM modelling.

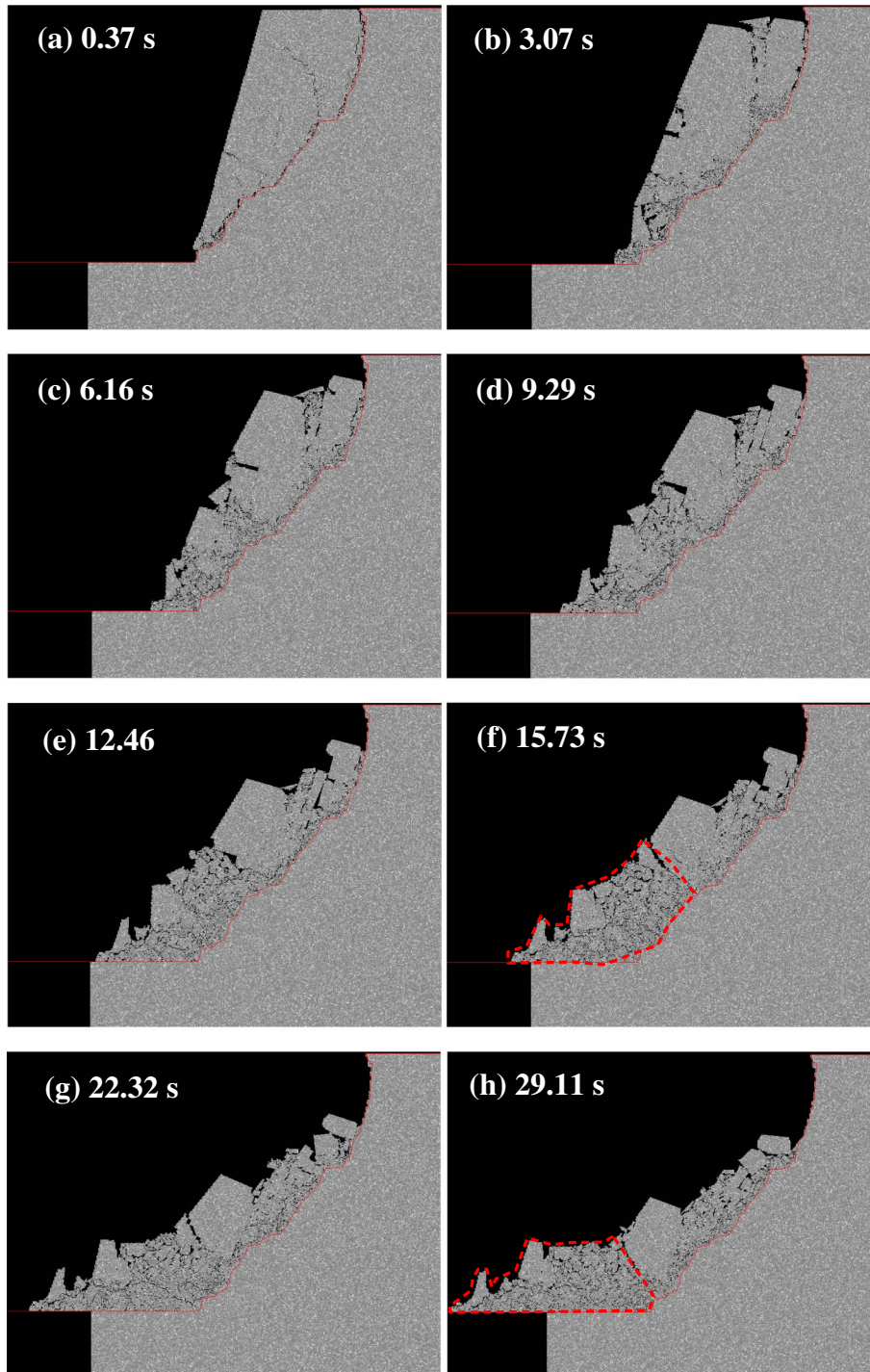


Fig. 16. Images showing block movement, rotation, and fracturing processes during the post-failure displacement of a slope with an initial slope angle $\alpha = 75^\circ$ at different time increments (from 0.37 to 29.11 s). Solid red lines delineate the sliding surface. The dashed red line in (f) shows the zone of broken, smaller blocks (see text for details). The dashed red line in (h) shows the fragmental nature of the forefront of the sliding region (for comparison with Fig. 17(d); see text for details). (For interpretation of the references to colour in this figure legend, the reader is referred to the web version of this article.)

FE modelling (shown in Fig. 12), and their accumulation is the main reason for the position of the slip surface. Many small blocks slide or roll together as post-failure slope deformation continues, accompanied by fragmentation of large blocks. Because the slip surface (red solid line in Fig. 16) is not smooth (same as on-site or experimental observation) and the blocks move against each other, the velocities of movement of those blocks are different from one another, which leads to the rolling of blocks. Furthermore, such

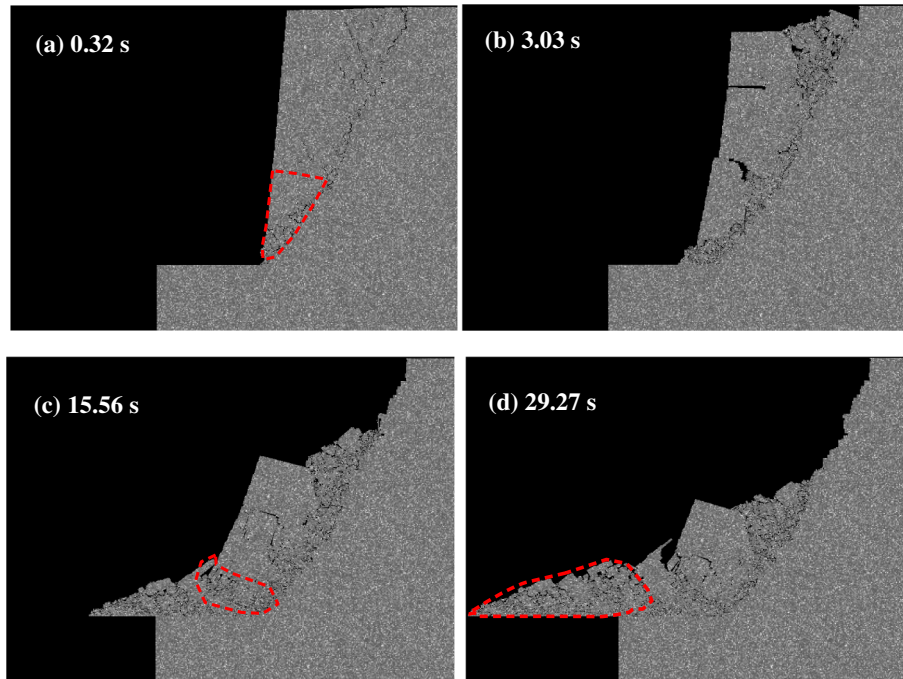


Fig. 17. Images showing block movement, rotation, and fracturing processes during the post-failure displacement of a slope with an initial slope angle $\alpha = 85^\circ$ at different time increments (from 0.32 to 29.27 s). Solid red lines delineate the sliding surface. The dashed red line in (d) shows the fragmental nature of the forefront of the sliding region (for comparison with Fig. 16(h); see text for details). (For interpretation of the references to colour in this figure legend, the reader is referred to the web version of this article.)

mechanical behaviour also results in joint failure during the landslide processes, subsequently forming smaller blocks, as shown in Fig. 16(d)–(f), in the forefront of landslide zone (indicated by the red dashed line in (f)). This phenomenon agrees with the failure characteristics of slopes with large slope angles. Finally, because of large gravitational loading, the sliding mass moves far from its original position, as shown in Fig. 16(h).

Fig. 17 shows the post-failure process of a slope with $\alpha = 85^\circ$. The most notable difference between $\alpha = 75^\circ$ and $\alpha = 85^\circ$ is that the fragments at the forefront of the sliding region in the slope with $\alpha = 85^\circ$ are smaller than those in slope with $\alpha = 75^\circ$ (see the zone within the red dashed line in Figs. 16(h) and 17(d)). The reason for this result lies in the fact that most of the gravity of the overlying sliding mass loads the mass at the toe of the slope (red dashed region shown in Fig. 17(a)) if the slope angle is large, but such a load is mostly supported by the rigid region in the slope with a small slope angle. During the landslide process, the movement of blocks adjacent to the contact between the sliding region and the rigid region results in block fragmentation at the contact zone, as shown by the red dashed zone shown in Fig. 17(c). The results also indicate that the sliding distance is longer when the slope angle is higher (at the same time following slip surface initiation).

The failures during the FE modelling stage are considered in the modelling of the sliding process by the DDA module, as shown in Figs. 16 and 17. In the classic DDA modelling, most studies did not consider failures during the initiation of the slip surface. To study the effect of such failures on the characteristics of the landslide, the following simulation of a landslide by the DDA module assumes that the input parameters (friction angle, cohesion and tensile strength) of the joints on the sliding surface are zero, and other joints in the sliding region (shown in Fig. 15) are consistent with the initial values of the elements, i.e., the joints at the edges of failed elements are not set to zero but are equal to the initial parameters of such elements. The modelling result is shown in Fig. 18, where the slope angle is 75° . It can be observed that the integrated sliding region slides along the sliding surface during the initial stages of post-failure slope deformation. Because of the roughness of the slip surface, the sliding region is broken into many large blocks, which differs from results with a homogeneous slip surface [10]. During the movement of the blocks, the larger ones can be split again and generate smaller blocks, as shown in Fig. 18(f)–(g) for the splitting process of block ①. Furthermore, similar to that shown in Fig. 16, block fragmentation is most efficient near the boundary between the sliding region and rigid region.

The advantages of the combined FEM and DDA method in handling static failure and post-failure behaviour of the slope are clearly noted in the discussion presented above. For both small and large displacements, the automatic identification of the slip surface, fragmentation, block movement, and rotation are easily addressed by the combined method. This is because the continuum-based finite element method has the advantage of static crack initiation, propagation, and coalescence modelling, including localization of failures, and the discontinuous failure along the slip surface of the sliding block is simulated without any difficulties by the DDA method.

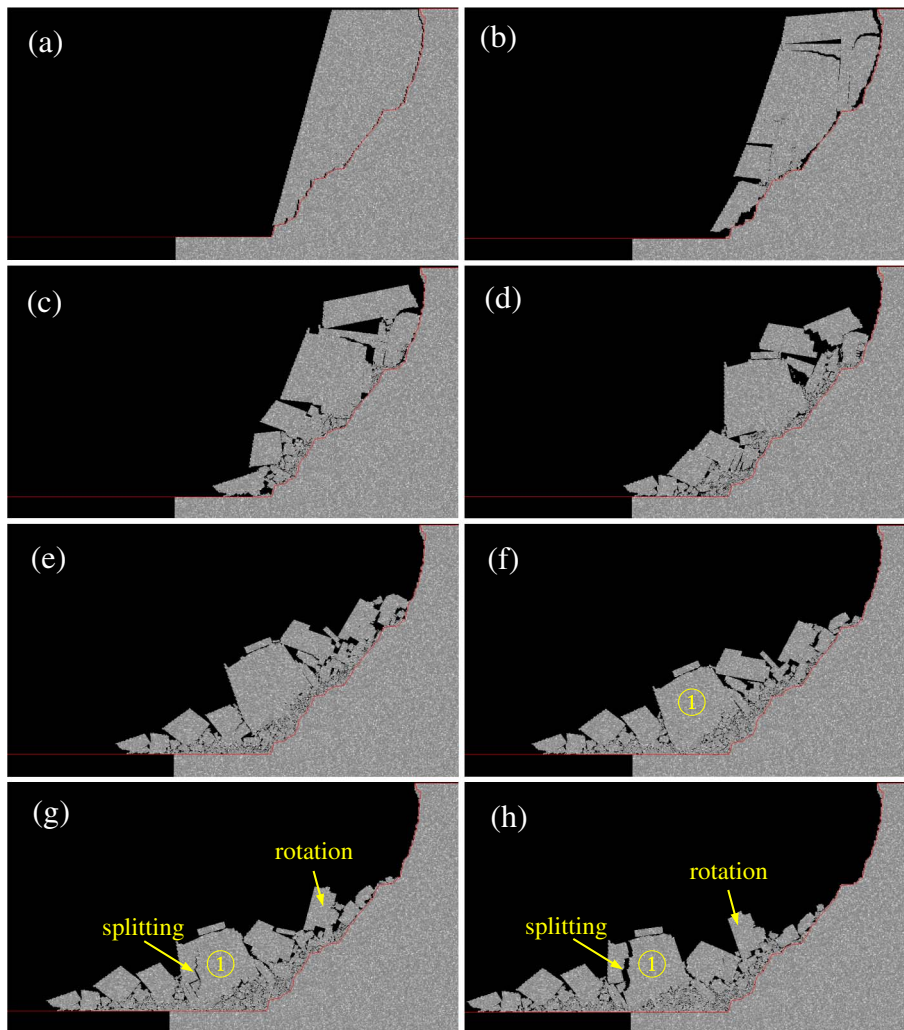


Fig. 18. Images showing block movement, rotation, and fracturing processes during the post-failure displacement of a slope with an initial slope angle $\alpha = 75^\circ$ without consideration of the element failure in the DDA modelling (see text for details). Solid red lines delineate the sliding surface. Block splitting and rotation are indicated in panels (g) and (h) (see text for details). (For interpretation of the references to colour in this figure legend, the reader is referred to the web version of this article.)

4. Conclusions

The progressive failure of a rock slope requires both continuous and discontinuous modelling. The continuous modelling must address the initiation, propagation and coalescences of cracks and automatically identify the slip surface of the slope. The discontinuous modelling should be able to simulate the block movement and rotation, block contact, fragmentation and large displacements. To realistically model such a complicated process, the combined FEM and DDA method offers a comprehensive analysis approach that is described in detail in this study. This proposed method is able to account for cracks or discontinuities within the slope and replicate the processes of crack propagation and coalescence. The failure mechanism of the slope, including crack initiation, propagation, and coalescence processes and post-failure characteristics, are studied, and the salient conclusions are stated as follows.

- (1) The proposed independent module method for slope stability studies that combines the FEM and DDA methods is simple in concept, and the combined scheme is easy to implement. We note that the FEM and DDA modules, and the transition from one module to the other, do not suffer any convergence problems. The limitation of this method, however, is that it can only model the slope instability in one step rather than segmented instability, which is more suitable for most rock slopes. Further development of this method should address more complex slope failure.
- (2) At the initial stage of slope failure, gravity induces small deformations manifest as crack initiation, propagation and coalescence. Shear cracks initiate near the toe of slope at first and then propagate upward along the slope. The classic viewpoint of failure at the toe of slope is that it only includes shear fractures. However, according to fracture mechanics, the initiation of shear cracks

results in large tensile stress that accumulates at the crack tips and further accelerates crack extension, i.e., both tensile and shear failures occur at this region. When the slip surface is formed, shear fractures may continue to occur, but tensile fracture is the main type of failure in the slope, especially in the region of the top surface.

- (3) The mechanical behaviours of the post-failure slope include blocks that slide or roll together, accompanied by fragmentation of large blocks. Most of the small blocks form and accumulate along the slip surface, which is attributed to the interaction between the sliding region and the rigid region. The size of the fragments at the forefront of the sliding region in a slope with a larger slope angle is smaller than that in a slope with a small slope angle. However, the slide distance in a slope with larger slope angle is longer than that with a low slope angle at the same time following slip surface initiation.
- (4) The failures initiated during formation of the slip surface significantly influence the post-failure mechanical behaviour. Pre-initiated cracks reduce the integrity of the sliding region and accumulate stress at their tips, which leads to a large number of small fragments during the sliding process. However, if these cracks are not considered during large displacement modelling, the integrated sliding region first slides along the sliding surface and is subsequently broken into many large blocks. Small fragments are only distributed near the contact zones between the sliding region and the rigid region.

This study advances insight into the failure process and the micro-failure mechanisms of slopes. This technique appears promising and complementary to those used in other cases for the simulation of slope evolution in heterogeneous materials. However, the application of this method to more realistic rock slope cases still requires further assessment and will be the subject of future work.

Acknowledgments

This project was financially supported by the National Basic Research Program of China (973 Program, Grant No. 2014CB047100), the National Natural Science Foundation of China (51421064, 51474046), the Opening Fund of State Key Laboratory of Geohazard Prevention and Geoenvironment Protection (Chengdu University of Technology) (SKLGP2014K017) and the Fundamental Research Funds for the Central Universities (DUT17LK35). M.J. Heap acknowledges a Visiting Erskine Fellowship from the University of Canterbury (New Zealand).

References

- [1] D.B. Kirschbaum, R. Adler, Y. Hong, S. Hill, A. Lerner-Lam, A global landslide catalog for hazard applications: method, results, and limitations, *Nat. Hazards* 52 (2010) 561–575.
- [2] D. Petley, Global patterns of loss of life from landslides, *Geology* 40 (2012) 927–930.
- [3] R. Huang, Understanding the mechanism of large-scale landslides, in: G. Lollino, D. Giordan, B.G. Crosta, J. Corominas, R. Azzam, J. Wasowski, N. Sciarra (Eds.), *Engineering Geology for Society and Territory - Volume 2: Landslide Processes*, Springer International Publishing, Cham, 2015, pp. 13–32.
- [4] I.G. Fourniadis, J.G. Liu, P.J. Mason, Landslide hazard assessment in the Three Gorges area, China, using ASTER imagery: Wushan–Badong, *Geomorphology* 84 (2007) 126–144.
- [5] M. Jiang, T. Jiang, G.B. Crosta, Z. Shi, H. Chen, N. Zhang, Modeling failure of jointed rock slope with two main joint sets using a novel DEM bond contact model, *Eng. Geol.* 193 (2015) 79–96.
- [6] G.B. Crosta, S. Imposimato, D.G. Roddeman, Numerical modelling of large landslides stability and runoff, *Nat. Hazards Earth Syst. Sci.* 3 (2003) 523–538.
- [7] D.V. Griffiths, P.A. Lane, Slope stability analysis by finite elements, *Geotechnique* 49 (1999) 387–403.
- [8] W.G. Pariseau, S.C. Schmelzer, A.K. Sheik, Mine slope stability analysis by coupled finite element modeling, *Int. J. Rock Mech. Min. Sci.* 34 (1997) (520–520).
- [9] F. Tschuchnigg, H.F. Schweiger, S.W. Sloan, Slope stability analysis by means of finite element limit analysis and finite element strength reduction techniques. Part I: numerical studies considering non-associated plasticity, *Comput. Geotech.* 70 (2015) 169–177.
- [10] H.H. Bui, R. Fukagawa, K. Sako, J.C. Wells, Slope stability analysis and discontinuous slope failure simulation by elasto-plastic smoothed particle hydrodynamics (SPH), *Geotechnique* 61 (2011) 565–574.
- [11] E. Hoek, C. Carranza-Torres, B. Corkum, Hoek-Brown failure criterion-2002 edition, *Proceedings of NARMS-Tac*, 1 2002, pp. 267–273.
- [12] P.A. Cundall, O.D.L. Strack, A discrete numerical model for granular assemblies, *Geotechnique* 29 (1979) 47–65.
- [13] G.H. Shi, Discontinuous deformation analysis: a new numerical model for the statics and dynamics of deformable block structures, *Eng. Comput.* 9 (1992) 157–168.
- [14] D. Stead, E. Eberhardt, J.S. Coggan, Developments in the characterization of complex rock slope deformation and failure using numerical modelling techniques, *Eng. Geol.* 83 (2006) 217–235, <http://dx.doi.org/10.1016/j.enggeo.2005.06.033>.
- [15] E. Eberhardt, D. Stead, J.S. Coggan, Numerical analysis of initiation and progressive failure in natural rock slopes—the 1991 Randa rockslide, *Int. J. Rock Mech. Min. Sci.* 41 (2004) 69–87.
- [16] L.N.Y. Wong, Z. Wu, Application of the numerical manifold method to model progressive failure in rock slopes, *Eng. Fract. Mech.* 119 (2014) 1–20.
- [17] Y.J. Ning, X.M. An, G.W. Ma, Footwall slope stability analysis with the numerical manifold method, *Int. J. Rock Mech. Min. Sci.* 48 (2011) 964–975.
- [18] G. Zhang, Y. Zhao, X. Peng, Simulation of toppling failure of rock slope by numerical manifold method, *Int. J. Comput. Methods* 7 (2010) 167–189.
- [19] R. Tian, L. Wen, Improved XFEM—an extra-dof free, well-conditioning, and interpolating XFEM, *Comput. Methods Appl. Mech. Eng.* 285 (2015) 639–658.
- [20] H. Bao, Z. Zhao, Modeling brittle fracture with the nodal-based discontinuous deformation analysis, *Int. J. Comput. Methods* 10 (2013) 1350040.
- [21] Y.M. Cheng, Y.H. Zhang, Coupling of FEM and DDA methods, *Int. J. Geomech.* 2 (2002) 503–517.
- [22] K. Shyu, Nodal-based Discontinuous Deformation Analysis, University of California, Berkeley, 1993.
- [23] L.Q. Choo, Z. Zhao, H. Chen, Q. Tian, Hydraulic fracturing modeling using the discontinuous deformation analysis (DDA) method, *Comput. Geotech.* 76 (2016) 12–22.
- [24] G.B. Crosta, F. Agliardi, Failure forecast for large rock slides by surface displacement measurements, *Can. Geotech. J.* 40 (2003) 176–191.
- [25] M. Debella-Gilo, A. Kääh, Measurement of surface displacement and deformation of mass movements using least squares matching of repeat high resolution satellite and aerial images, *Remote Sens.* 4 (2012) 43–67.
- [26] G.J. Dick, E. Eberhardt, A.G. Cabrejo-Liévano, D. Stead, N.D. Rose, Development of an early-warning time-of-failure analysis methodology for open-pit mine slopes utilizing ground-based slope stability radar monitoring data, *Can. Geotech. J.* 52 (2014) 515–529.
- [27] C.A. Tang, S.B. Tang, Applications of rock failure process analysis (RPPA) method, *J. Rock Mech. Geotech. Eng.* 3 (2011) 352–372.
- [28] S.B. Tang, C.A. Tang, Crack propagation and coalescence in quasi-brittle materials at high temperatures, *Eng. Fract. Mech.* 134 (2015) 404–432.

- [29] K. Terzaghi, Stability of steep slopes on hard unweathered rock, *Geotechnique* 12 (1962) 251–270.
- [30] H.H. Einstein, D. Veneziano, G.B. Baecher, K.J. O'reilly, The effect of discontinuity persistence on rock slope stability, *Int. J. Rock Mech. Min. Sci. Geomech. Abstr.* 20 (1983) 227–236.
- [31] L. Scholtès, F.V. Donzé, A DEM analysis of step-path failure in jointed rock slopes, *Comptes Rendus Mecanique* 343 (2015) 155–165.
- [32] P.J.N. Pells, Uniaxial strength testing, *Comprehensive Rock Engineering*, Pergamon Press, Oxford, 1993.
- [33] L. Griffiths, M.J. Heap, T. Xu, C.F. Chen, P. Baud, The influence of pore geometry and orientation on the strength and stiffness of porous rock, *J. Struct. Geol.* 96 (2017) 149–160.
- [34] M.J. Heap, F.B. Wadsworth, T. Xu, C.F. Chen, The strength of heterogeneous volcanic rocks: a 2D approximation, *J. Volcanol. Geotherm. Res.* 319 (2016) 1–11.
- [35] T.F. Wong, R.H.C. Wong, K.T. Chau, C.A. Tang, Microcrack statistics, Weibull distribution and micromechanical modeling of compressive failure in rock, *Mech. Mater.* 38 (2006) 664–681.
- [36] S.B. Tang, H. Zhang, C.A. Tang, H.Y. Liu, Numerical model for the cracking behavior of heterogeneous brittle solids subjected to thermal shock, *Int. J. Solids Struct.* 80 (2016) 520–531.
- [37] C.C. Swan, Y.K. Seo, Limit state analysis of earthen slopes using dual continuum/FEM approaches, *Int. J. Numer. Anal. Methods Geomech.* 23 (1999) 1359–1371.
- [38] T. Mateui, K.C. San, Finite element slope stability analysis by shear strength reduction, *Soils Found.* 32 (1992) 59–70.
- [39] G.H. Shi, R.E. Goodman, Two dimensional discontinuous deformation analysis, *Int. J. Numer. Anal. Methods Geomech.* 9 (1985) 541–556.
- [40] G. Zhang, A.X. Wang, T.P. Mu, J.M. Zhang, Study of stress and displacement fields in centrifuge modeling of slope progressive failure, *Rock Soil Mech.* 29 (2008) 2637–2641.
- [41] Y. Hu, G. Zhang, J.M. Zhang, C.F. Lee, Centrifuge modeling of geotextile-reinforced cohesive slopes, *Geotext. Geomembr.* 28 (2010) 12–22.
- [42] L. Jing, Formulation of discontinuous deformation analysis (DDA)—an implicit discrete element model for block systems, *Eng. Geol.* 49 (1998) 371–381.